A Semi-Automatic Method for Road Centerline Extraction From VHR Images

Zelang Miao, Bin Wang, Wenzhong Shi, and Hua Zhang

***Abstract*—This letter presents a semi-automatic approach to delineating road networks from very high resolution satellite images. The proposed method consists of three main steps. First, the geodesic method is used to extract the initial road segments that link the road seed points prescribed in advance by users. Next, a road probability map is produced based on these coarse road segments and a further direct thresholding operation separates the image into two classes of surfaces: the road and nonroad classes. Using the road class image, a kernel density estimation map is generated, upon which the geodesic method is used once again to link the foregoing road seed points. Experiments demonstrate that this proposed method can extract smooth correct road centerlines.**

***Index Terms*—Kernel density estimation (KDE), geodesic method, mean shift, road extraction, semi-automatic, very high resolution (VHR) satellite images.**

I. Introduction

VERY high resolution (VHR) satellite images have become increasingly available in recent years with the advent of modern acquisition sensors such as SPOT, IKONOS, and WorldView-2. These sensors produce massive streams of images; hence, image interpretation and analysis are required to process them. Road extraction from VHR satellite images is an important image processing technology that has many vital applications such as updating of transportation databases, urban planning, and change detection. Road delineation has received much attention over the years, and various methods have been proposed for achieving this task. In general, road classification methods can be classified into two categories [1], [2]: fully automatic and semi-automatic. Although fully automatic methods have been researched for many years, their results have been generally discouraging due to various negative factors (i.e., image noise, occlusion of trees, and shadows) [3]. Therefore, full automation remains elusive and fragile [4], and this letter focuses on developing a semi-automatic road extraction method.

Road extraction methods have been founded on diverse image processing technologies, including ridge detection [2], [5], image classification and segmentation [6]–[11], or snakes [12]. The integration of spectral and spatial signatures has also been investigated as a means to extract road features [7]–[10], [13]. This integrated method has shown relatively better performance than methods that only use spectral information. Hu *et al.* [14] presented a robust semi-automated method for road centerline delineation in which the piecewise parabola model was constructed around seed points provided by users. Least squares template matching was subsequently applied to compute the parabola parameters. Similarly, Lin *et al.* [15] presented a semi-automatic extraction of road networks by using a least squares interlaced template matching method. Comprehensive summaries on these state-of-the-art road extraction methods have been compiled by Mena [1] and Das *et al.* [2].

This letter proposes a semi-automatic method for road delineation from VHR satellite images. The proposed method is an extension of the geodesic method [16] in which low spatial resolution images are processed. Although the previous integrated method shows certain advantages in processing low spatial resolution images, it is not suitable for VHR images. The proposed method solves this limitation. The remainder of this letter is organized as follows. Section II presents the basic principles of the proposed method. Preliminary results are reported in Section III, and conclusions are discussed in Section IV.

II. Methodology

A. Geodesic Method

In this letter, the geodesic method [16] is selected to link seed points and identify the central line for roadways. Let f denote the probability density estimation map, which is modeled as a 2-D function $f : \Omega \to \mathbb{R}$. The image domain Ω is usually defined as $\Omega = [0, 1]^2$. In road linking, a road that connects two seed points $\boldsymbol{x}_s$ and $\boldsymbol{x}_e$ can be approximately defined as a smooth curve that has a constant gray value $c \in \mathbb{R}$. Based on this definition of road model, a saliency map $W(\cdot)$ at the pixel $\boldsymbol{x}$ is then defined as

$$W(\boldsymbol{x}) = |f(\boldsymbol{x}) - c| + \varepsilon \tag{1}$$

where ε (i.e., $\varepsilon = 0.01$) is a small value that prevents $W(\boldsymbol{x})$ from vanishing, and c is the gray value at the start point $\boldsymbol{x}_s$ (i.e.,

Manuscript received December 26, 2013; revised February 16, 2014 and March 12, 2014; accepted March 12, 2014. Date of publication April 8, 2014; date of current version May 22, 2014. This work was supported in part by the National Natural Science Foundation of China under Grant 41201451 and Grant 40901214 and in part by the Ministry of Science and Technology of China under Project 2012BAJ15B04 and Project 2012AA12A305.

Z. Miao is with the Department of Land Surveying and Geo-Informatics, Hong Kong Polytechnic University, Kowloon, Hong Kong and also with the School of Environmental Science and Spatial Informatics, China University of Mining and Technology, Xuzhou 221116, China.

B. Wang is with the Department of Land Surveying and Geo-Informatics, Hong Kong Polytechnic University, Kowloon, Hong Kong.

W. Shi is with the Department of Land Surveying and Geo-Informatics, Hong Kong Polytechnic University, Kowloon, Hong Kong and also with Wuhan University, Wuhan 430072, China (e-mail: lswzshi@polyu.edu.hk).

H. Zhang is with the School of Environmental Science and Spatial Informatics, China University of Mining and Technology, Xuzhou 221116, China.

Color versions of one or more of the figures in this paper are available online at http://ieeexplore.ieee.org.

Digital Object Identifier 10.1109/LGRS.2014.2312000

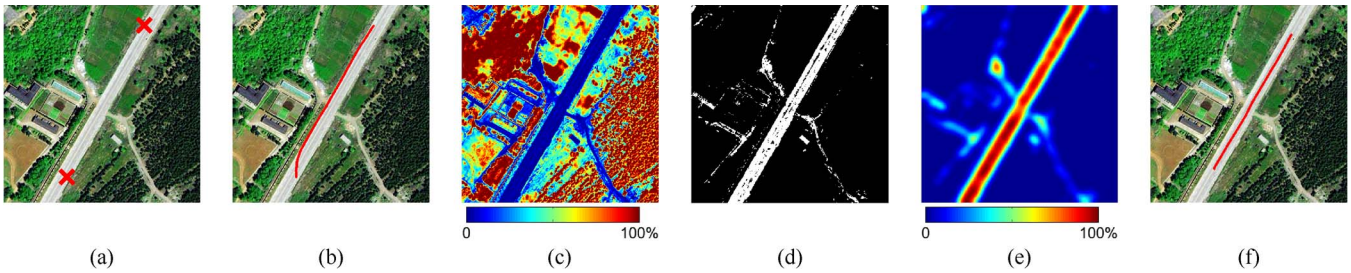

Fig. 1. (a) Test image where seed points are shown in blue crosses. (b) Minimal path extracted by the geodesic method shown in red. (c) Mahalanobis distance map. (d) Thresholding result, in which 1 and 0 represent *road* and *nonroad* class, respectively. (e) Result of kernel density estimation. (f) Minimal path extracted by repeating the geodesic method on the KDE result.

$c = f(\boldsymbol{x}_s)$). According to (1), the area through which the road passes should have low values of $W(\boldsymbol{x})$. Based on the saliency map, the length of a smooth curve on the image $\gamma : [0,\ 1] \to \Omega$ is defined as a weighted length as follows:

$$L(\gamma) = \int_0^1 W\left(\gamma(t)\right) \left\|\gamma'(t)\right\| \, dt \tag{2}$$

where $\gamma'(t) \in \mathbb{R}^2$ is the derivative of γ. For linking road seed points, γ is generally constrained by

$$\left\{\gamma : [0,\ 1] \to \Omega \setminus \gamma(0) = \boldsymbol{x}_s \quad \text{and} \quad \gamma(1) = \boldsymbol{x}_e\right\}. \tag{3}$$

The minimal path γ^* is defined as

$$\gamma^* = \underset{\gamma \in (\boldsymbol{x}_s, \boldsymbol{x}_e)}{\arg\min}\ L(\gamma). \tag{4}$$

The geodesic path is computed on the gray image, which cannot be applied directly to the multispectral image. There are many algorithms to tackle this limitation, such as spectral angle and principal component analysis transformation. For ease of computation in this letter, multispectral satellite images are first summed and averaged to obtain a single band image. The experimental results show that this simple step is sufficient. The geodesic method is subsequently applied to the averaged image for extracting the minimal path between seed points. An example of the geodesic method is depicted in Fig. 1. It can be seen that this method can correctly infer the spatial connection, and there is no need to guarantee the spatial connection topology. A well-recognized problem for the geodesic method is that of bias. Fig. 1(b) illustrates such a problem, showing a minimal path that tends to follow the boundary of the road but does not coincide with the true centerline. This limitation must be considered, and the proposed method for dealing with such issues is described in the following.

B. Road Probability Estimation

The initial road segments generated by the geodesic method are taken as training samples. Then, we use the Mahalanobis distance [17] to measure the probability of a pixel $\boldsymbol{x}$ being of the *road* class, as follows:

$$p_M(\boldsymbol{x}) = \sqrt{\left(I(\boldsymbol{x}) - \mu\right)^T S^{-1} \left(I(\boldsymbol{x}) - \mu\right)} \tag{5}$$

where μ and S denote the mean value and the covariance matrix of training samples, respectively, and $I(\boldsymbol{x})$ is the spectral value at the pixel $\boldsymbol{x}$. Using the Mahalanobis distance to compute the road probability is valid as this measure is unitless and efficient to compute. After the computation of the road probability map, a simple thresholding is applied to segment the images into two classes: *road* class and *nonroad* class. The thresholding result is defined as

$$\mathrm{CL}(\boldsymbol{x}) = \begin{cases} 1, & \text{if } p_M(\boldsymbol{x}) \le \text{threshold} \\ 0, & \text{otherwise} \end{cases} \tag{6}$$

where $\mathrm{CL}(\boldsymbol{x})$ is the class label of the pixel $\boldsymbol{x}$, the threshold value is automatically obtained by Otsu's method [18], and 1 and 0 represent the *road* class and *nonroad* class, respectively. Fig. 1(c) and (d) shows the Mahalanobis distance matrix and its corresponding thresholding result, respectively. Although the thresholding method misclassifies some road pixels, this error has little influence on the accuracy of the road centerline extraction as the connection of seed points in the proposed method relied on the geodesic method, which is robust to noise.

C. KDE and Mean Shift

After the road probability estimation, KDE technology [19] is introduced to assess the probability that any given pixel lies on the road centerline. Let $y_1, y_2, \ldots, y_n$ be a given set of d-dimensional random samples. The kernel density estimator is defined as

$$\hat{f}(y) = \frac{1}{nh^d} \sum_{i=1}^{n} K\left(\frac{y - y_i}{h}\right) \tag{7}$$

where n is the number of observations, h denotes the bandwidth parameter (which is determined by generalizing Scott's rule of thumb [19]), and K is the kernel function. We selected the Gaussian kernel as the kernel function as follows:

$$K(y) = e^{-\frac{y^2}{2h^2}}. \tag{8}$$

An example of a KDE result is shown in Fig. 1(e). It can be seen that pixels on road centerlines have higher KDE values than pixels that are uncentered. It is worth pointing out that seed points selected by users may not precisely locate on road centerlines, and this factor affects the accuracy of the minimal path. To achieve robustness to such distortions, we rely on the mean shift method [20] to obtain precise centered positions of

seed points. Mean shift, a procedure to iteratively detect modes of the kernel function, has the following generic formula:

$$m(y) = \frac{\sum_{i=1}^{n} g\left(\frac{y-y_i}{h}\right) y_i}{\sum_{i=1}^{n} g\left(\frac{y-y_i}{h}\right)} - y \tag{9}$$

where $g(y) = -K'(y)$. After projecting road seed points onto the ridge through KDE, the geodesic method is repeated to trace road centerlines using the KDE map, with the result shown in Fig. 1(f). It can be seen that the proposed method enables us to obtain the centered result.

As discussed earlier, the procedures of the proposed method are summarized in **Algorithm 1**.

Algorithm 1 Linking of seed points using the proposed method

1. Manually label seed points on the input satellite image.
2. Extract the minimal path between seed points using the geodesic method.
3. Compute the road probability map using the Mahalanobis distance, in which training samples consist of pixels that locate on the minimal path produced by Step 2.
4. Segment the Mahalanobis distance map by applying a simple thresholding.
5. Apply KDE to compute the probability that a pixel locates on the centerline.
6. Project seed points onto the ridge of the KDE.
7. Based on the KDE map, repeat the geodesic method to extract the minimal path between seed points.

III. Experiments

A. Tests on Sensitivity of Seed Positions

To demonstrate the performance of the proposed method, an aerial image with a spatial resolution of 0.3 m/pixel was tested, and the geodesic method was selected as the reference method. The results are shown in Fig. 2. As can be observed, the proposed method could provide better results than the geodesic method. The experimental results show that the original geodesic method was sensitive to the positions of seed points, in that different positions for the seed points produced different road centerlines. Thus, the original geodesic method was less robust. Fig. 2(b) also shows that road centerlines produced by the original geodesic path method were wrongly extracted. In particular, although the seed points were located at centerlines, the original geodesic method still could not achieve correct results. In contrast, the proposed method was insensitive to the positions of seed points and could achieve reliable accurate road centerlines. The proposed method is more accurate as it has two advantages. First, the mean shift can project initial seed points onto the ridge of the KDE. Second, the geodesic path using KDE traces the road centerline along the ridge line. Furthermore, a visual comparison of the results in Fig. 2 evidently validates the advantage of the proposed method in road centerline extraction. The poor performance of the original geodesic approach demonstrates its inability to extract road centerlines from VHR satellite images. However, as suggested earlier, the proposed method solves the limitation of the geodesic method and provides a practical solution for the road centerline extraction.

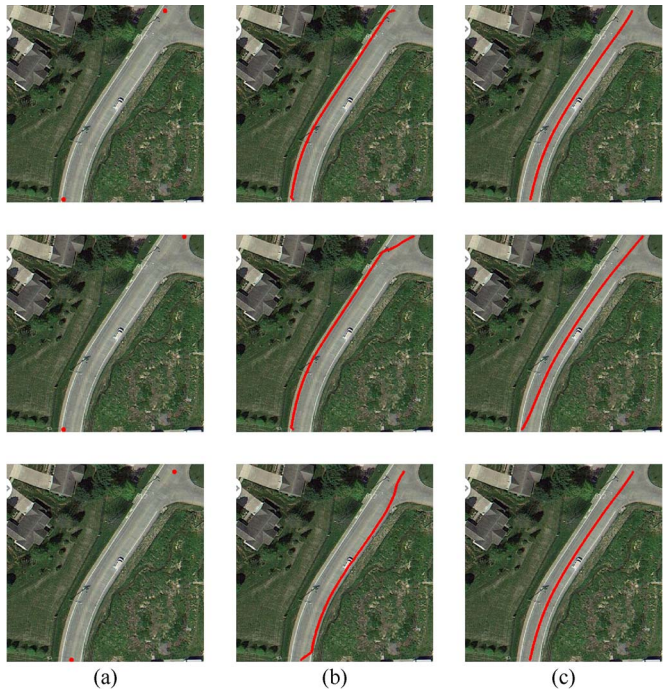

Fig. 2. Comparison of road centerline extraction results. (a) Original images with different seed points shown in red circles. (b) Results by the geodesic method. (c) Results by the proposed method. The centerline results are shown in red.

B. Experiments

A QuickBird image downloaded from VPLab [21] was used to evaluate the proposed method. The study area had a spatial size of 512 × 512 pixels. The satellite image used in this letter had a spatial resolution of 0.6 m/pixel. Fig. 3(a) shows the study area in which the seed points selected by users are shown in blue crosses. The geodesic method was first applied to obtain the minimal path that linked seed points, with the results shown in Fig. 3(b). Finally, the proposed method is depicted in Fig. 3(c). A comparison of the two methods is presented in Fig. 3(d). As shown, the result of the proposed method is more centered than that of the geodesic method. Hence, the proposed method more accurately extends the geodesic method to extract road centerlines from VHR images.

In the second experiment, an image with a spatial size of 400 × 400 pixels, downloaded from [22], was used to test the proposed method's performance. Fig. 4(a)–(c) shows the test image, the geodesic method result, and the proposed method result, respectively. It is shown that both the geodesic method and the proposed method can achieve results with the desired "U" shape. However, the result of the proposed method is more centered than that of the geodesic method.

The road extraction result for the third test image was obtained using another QuickBird image downloaded from VPLab [21]. This test image, with a spatial size of

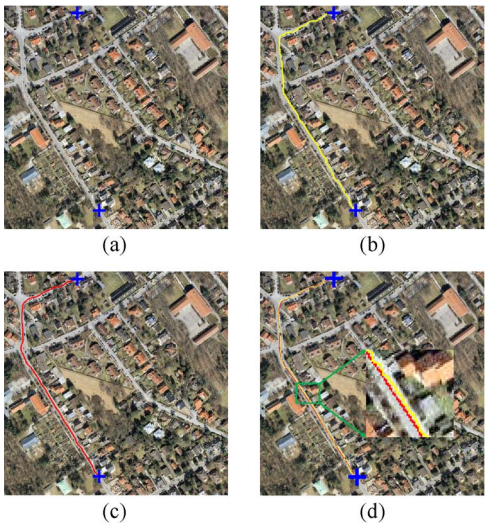

Fig. 3. Results on the first image. (a) Test image where seed points are shown in blue crosses. (b) Geodesic method result shown in yellow. (c) Proposed method result shown in red. (d) Comparison results of two methods, where the geodesic method and the proposed method are shown in yellow and red, respectively.

Fig. 4. Results on the second image. (a) Test image in which seed points are shown in blue crosses. (b) Geodesic method result shown in yellow. (c) Proposed method result shown in red.

Fig. 5. Results on the third image. (a) Test image in which seed points are shown in blue crosses. (b) Geodesic method result shown in yellow. (c) Proposed method result shown in red.

512×512 pixels, is shown in Fig. 5(a). It is shown that two seed points are located in regions with different materials. In other words, the gray values of the two seed points are significantly different. The road connection results of the geodesic method and the proposed method are shown in Fig. 5(b) and (c), respectively. These results show that both methods failed to extract roads with the desired topology. It seems that the long detour necessary for the true solution plays a significant role. Therefore, the limitation of the proposed method is that it fails in a situation of material change. A possible solution to this problem would be to use the object space method, based on intensity-change-invariant road shape features.

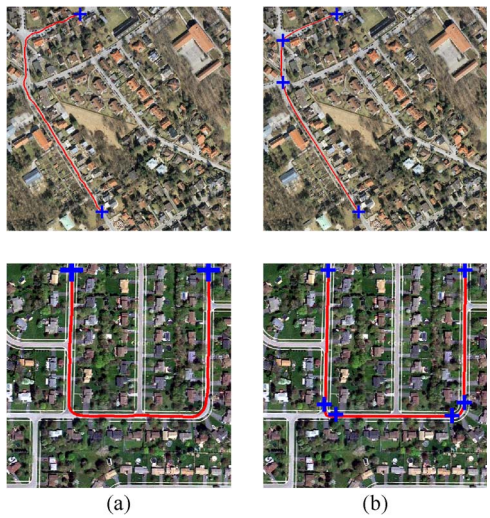

Fig. 6. Comparison with the existing semi-automatic method. (a) Proposed method results shown in red. (b) Results produced by Hu *et al.* [14] shown in red. Seed points are shown in blue crosses.

TABLE I
COMPARISON OF TWO SEMI-AUTOMATIC ROAD CENTERLINE EXTRACTION METHODS

	Proposed method	Hu's method
Experiment 1		
Number of seed points	2	4
Total road length	520	487
Completeness (%)	96.54	96.77
Correctness (%)	96.54	98.47
Quality (%)	93.31	95.34
Experiment 2		
Number of seed points	2	6
Total road length	737	760
Completeness (%)	95.20	99.21
Correctness (%)	96.88	99.60
Quality (%)	92.37	98.81

C. Comparison With an Existing Method

The proposed method was compared with a semi-automatic road centerline extraction method drawn from the existing literature. Fig. 6 depicts the comparison results of the proposed method and the method used by Hu *et al.* [14]. This method was selected because it and the proposed method both rely on seed points selected by users, which guaranteed a fair comparison.

When quantifying the performance values, five accuracy measures [14], [23] were used to evaluate the semi-automatic centerline extraction methods. These measures were: 1) number of seed points; 2) total road length; 3) completeness $= \mathrm{TP}/(\mathrm{TP}+\mathrm{FN})$; 4) correctness $= \mathrm{TP}/(\mathrm{TP}+\mathrm{FP})$; and 5) quality $= \mathrm{TP}/(\mathrm{TP}+\mathrm{FP}+\mathrm{FN})$. The variables TP, FN, and FP denote true positive, false negative, and false positive, respectively. In this letter, the true road centerline between two seed points was provided by the hand drawing method, and the buffer width is fixed to eight pixels.

Table I shows the results of the two methods. It is shown that the proposed method and that proposed by Hu *et al.* achieved similar accuracy. However, the proposed method needed fewer

seed points than the Hu *et al.* method. Hu *et al.*'s method needed more seed points because it requires that seed points be labeled where the road curvature changes. Compared with Hu *et al.*'s method, the proposed method needed fewer interactions with users. Therefore, the proposed method shows a stronger global inference for connection of seed points than Hu *et al.*'s method. The experimental results indicate a great potential of the proposed method for practical delineation of roads from VHR satellite images.

IV. Conclusion

A semi-automatic method for road centerline extraction from VHR satellite images has been proposed in this letter. More specifically, the proposed method was shown to incorporate the strengths of the geodesic method, KDE, and mean shift. In contrast to the geodesic method, a combination of the geodesic method and KDE provided a better solution for tracing an unbiased road centerline between seed points. The application of the mean shift method allowed the proposed method to obtain precise seed points from coarse points selected by users. These versatile functions allowed us to extract robust road centerlines that were not subject to the positions of seed points that affect the geodesic method.

One of the immediate practical applications of the proposed method is that the road discontinuities of other road extraction algorithms can be eliminated. In its present form, the proposed method is semi-automatic and needs seed points that need to be manually selected. Future work will therefore focus on automatic selection of the road seed points, and on the use of graph theory for extracting a complete road network.

Acknowledgment

The authors would like to thank Prof. P. Gamba from the University of Pavia for the kind discussions on road extraction, and the Editor and two anonymous reviewers whose insightful suggestions and constructive comments have significantly improved this letter.

References

[1] J. B. Mena, "State of the art on automatic road extraction for GIS update: A novel classification," *Pattern Recognit. Lett.*, vol. 24, no. 16, pp. 3037–3058, Dec. 2003.

[2] S. Das, T. T. Mirnalinee, and K. Varghese, "Use of salient features for the design of a multistage framework to extract roads from high-resolution multispectral satellite images," *IEEE Trans. Geosci. Remote Sens.*, vol. 49, no. 10, pp. 3906–3931, Oct. 2011.

[3] A. P. Dal Poz, R. A. B. Gallis, J. F. C. da Silva, and E. F. O. Martins, "Object-space road extraction in rural areas using stereoscopic aerial images," *IEEE Trans. Geosci. Remote Sens.*, vol. 9, no. 4, pp. 654–658, Jul. 2012.

[4] E. Türetken, G. González, C. Blum, and P. Fua, "Automated reconstruction of dendritic and axonal trees by global optimization with geometric priors," *Neuroinformatics*, vol. 9, no. 2/3, pp. 279–302, Sep. 2011.

[5] R. Nevatia and K. Babu, "Linear feature extraction and description," *Comput. Graphics Image Process.*, vol. 13, no. 3, pp. 257–269, Jul. 1980.

[6] K. Treash and K. Amaratunga, "Automatic road detection in gray scale aerial images," *ASCE J. Comput. Civil Eng.*, vol. 14, no. 1, pp. 60–69, Jan. 2000.

[7] Z. Miao, W. Shi, H. Zhang, and X. Wang, "Road centerline extraction from high-resolution imagery based on shape features and multivariate adaptive regression splines," *IEEE Geosci. Remote Sens. Lett.*, vol. 10, no. 3, pp. 583–587, May 2013.

[8] W. Shi, Z. Miao, and J. Debayle, "An integrated method for urban main road centerline extraction from optical remotely sensed imagery," *IEEE Trans. Geosci. Remote Sens.*, vol. 52, no. 6, pp. 3359–3372, Jun. 2014.

[9] W. Shi, Z. Miao, Q. Wang, and H. Zhang, "Spectral-spatial classification and shape features for urban road centerline extraction," *IEEE Geosci. Remote Sens. Lett.*, vol. 11, no. 4, pp. 788–792, Apr. 2013.

[10] M. J. Song and D. Civco, "Road extraction using SVM and image segmentation," *Photogramm. Eng. Remote Sens.*, vol. 70, no. 12, pp. 1365–1371, Dec. 2004.

[11] J. Yuan, D. Wang, B. Wu, L. Yan, and R. Li, "LEGION-based automatic road extraction from satellite imagery," *IEEE Trans. Geosci. Remote Sens.*, vol. 40, no. 2, pp. 4528–4538, Nov. 2011.

[12] Y. Nakaguro, S. S. Makhanov, and M. N. Dailey, "Numerical experiments with cooperating multiple quadratic snakes for road extraction," *Int. J. Geogr. Inf. Sci.*, vol. 25, no. 5, pp. 765–783, May 2011.

[13] A. Grote, C. Heipke, and F. Rottensteiner, "Road network extraction in suburban areas," *Photogramm. Rec.*, vol. 27, no. 137, pp. 8–28, Mar. 2012.

[14] X. Hu, Z. Zhang, and C. V. Tao, "A robust method for semi-automatic extraction of road centerlines using a piecewise parabolic model and least square template matching," *Photogramm. Eng. Remote Sens.*, vol. 70, no. 12, pp. 1393–1398, Dec. 2004.

[15] X. Lin, J. Zhang, Z. Liu, J. Shen, and M. Duan, "Semi-automatic extraction of road networks by least squares interlaced template matching in urban areas," *Int. J. Remote Sens.*, vol. 32, no. 17, pp. 4943–4959, Sep. 2011.

[16] G. Peyré, M. Péchaud, R. Keriven, and L. D. Cohen, "Geodesic methods in computer vision and graphics," *Found. Trends Comput. Graphics Vis.*, vol. 5, no. 3/4, pp. 197–397, Mar. 2010.

[17] T. Hastie, R. Tibshirani, and J. Friedman, *The Elements of Statistical Learning: Data Mining, Inference, and Prediction,* 2nd ed. Berlin, Germany: Springer-Verlag, 2008.

[18] N. Otsu, "A threshold selection method from gray-level histograms," *IEEE Trans. Syst., Man, Cybern.*, vol. SMC-9, no. 1, pp. 151–172, Jun. 1979.

[19] I. Ahamada and E. Flachaire, *Non-Parametric Econometrics*. Oxford, U.K.: Oxford Univ. Press, 2010.

[20] Y. Cheng, "Mean shift, mode seeking, and clustering," *IEEE Trans. Pattern Anal. Mach. Intell.*, vol. 17, no. 8, pp. 790–799, Aug. 1995.

[21] VPLab, Downloads 2013. [Online]. Available: http://www.cse.iitm.ac.in/~sdas/vplab/satellite.html

[22] Computer Vision Lab, Data 2013. [Online]. Available: http://cvlab.epfl.ch/data/delin

[23] C. Wiedemann, C. Heipke, and H. Mayer, "Empirical evaluation of automatically extracted road axes," in *Proc. CVPR*, 1998, pp. 172–187.